Development of a dataset on the in-plane experimental response of URM piers with bricks and blocks

Morandi, P.; Albanesi, L.; Graziotti, F.; Li Piani, T.; Penna, A.; Magenes, G.

DOI
10.1016/j.conbuildmat.2018.09.070

Publication date
2018

Document Version
Accepted author manuscript

Published in
Construction and Building Materials

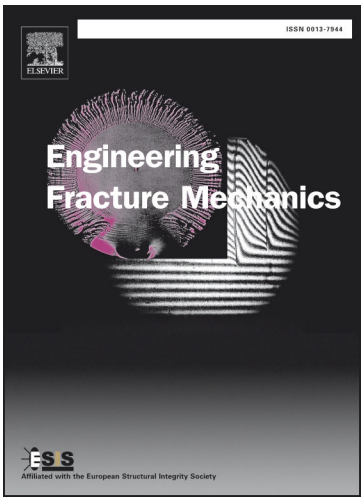

The Adobe Delta Damage Model: A locally regularized rate-dependent model for the static assessment of soil masonry bricks and mortar

T. Li Piani, J. Weerheijm, L. Koene, L.J. Sluys

PII: S0013-7944(18)30895-6
DOI: https://doi.org/10.1016/j.engfracmech.2018.11.026
Reference: EFM 6239

To appear in: *Engineering Fracture Mechanics*

Received Date: 31 August 2018
Accepted Date: 12 November 2018

Please cite this article as: Li Piani, T., Weerheijm, J., Koene, L., Sluys, L.J., The Adobe Delta Damage Model: A locally regularized rate-dependent model for the static assessment of soil masonry bricks and mortar, *Engineering Fracture Mechanics* (2018), doi: https://doi.org/10.1016/j.engfracmech.2018.11.026

The Adobe Delta Damage Model: A locally regularized rate-dependent model for the static assessment of soil masonry bricks and mortar

T. Li Piani[a,b,c,*], J. Weerheijm[a,c], L. Koene[b], L.J. Sluys[a]

[a] *TU Delft, Stevinweg 1, 2628 CN Delft, The Netherlands*
[b] *NLDA, Het Nieuwe Diep 8, NL-1781 CA Den Helder, The Netherlands*
[c] *TNO, PO Box 45, 2280 AA Rijswijk, The Netherlands*

Abstract

A local damage model is proposed for the numerical assessment of the static performance of Adobe masonry components. The model was applied to simulate the experimental behaviour of sundried soil bricks and mud mortar tested in uniaxial compression and bending. Numerical simulations of the model are made mesh objective by means of a rate dependent regularization algorithm in statics. This is achieved using a generalization of the damage delay concept based on a decomposition of the Dirichlet boundary condition. It allows non-dimensionality of model parameters mathematically needed to prevent loss of ellipticity of the equilibrium equations of the model. The entire regularization algorithm is integrated within an implicit Newton-Raphson solver.

Keywords: Adobe; delta; damage; mesh; dependence; rate; Dirichlet; boundary; compression; bending; brick; mortar; Mohr-Couloumb.

1. Introduction

The complexity of natural and man-made hazard scenarios in current society from which buildings in urban environments must be protected, requires the development of efficient interpretative tools [1, 2]. This task is translated in the

*Tiziano Li Piani
Email address: t.lipiani@tudelft.nl (T. Li Piani)

field of computational mechanics into the need for effective material and structural models which demonstrate numerical robustness, computational efficiency and physical consistency. Industry and research face a serious challenge when continuum damage mechanics is adopted to simulate the response of quasi brittle materials, such as concrete, commonly used for civil constructions. In fact, quasi brittle materials are typically characterized by softening behaviour, that is the slope of the post peak stress region is negative [3, 4]. This happens because the material is progressively degraded by the stemming and coalescence of internal microcracks bridging into macro-cracks [5, 6]. Interpreting failure as a progressive degradation of the elastic stiffness of the material, continuum damage mechanics constitutes a numerical approach conceptually close to the phenomenology of quasi brittle materials [4, 7]. However, this class of models suffers from a serious numerical pathology named mesh dependence [8]. That is, numerical simulations of softening materials result into localization of damage within the smallest area allowed by the spatial discretization of the material domain [9]. This happens because the boundary value problem becomes ill posed, due to loss of ellipticity of the governing equations of equilibium [3, 10]. As a consequence, results of numerical simulations using local damage models depend on the adopted discretization, both in terms of extension of failure regions and force displacement diagrams, depicting a progressively more brittle response upon mesh refinement.

Mesh sensitivity is a well known issue and several numerical treatments, defined as regularization methods, have been developed over the years [5]. All methods imply the introduction of localization limitizers (or length scale) in the local model, meant to prevent hyperbolicity of the equilibrium equations to occur and differently introduced according to the adopted strategy of regularization [11]. Unfortunately in most cases, these algorithms solve mesh dependence at the expense of the aforementioned requirements needed for an effective numerical model. The use of a nonlocal model is the most popular regularization method nowadays [3, 12]. The general principle is that the stress at a given integration point is not uniquely determined by the history of the strain at this point, but

also by the mutual interactions with nearby ones [13, 14]. Despite being usually effective in obtaining mesh objective simulations, nonlocal models often imply non standard code developments, difficult parameter identification procedures and inadequacies close to free boundaries, besides extra computational costs inherent to nonlocal models [15, 16]. As an alternative, gradient models may also be employed to solve mesh dependence. They prescribe enrichment of the equilibrium equations with extra gradients of the state variables to solve ill posedess of the boundary value problem. Similar to the use of non local models, numerical simulations using gradient models are often prone to a broadening of the damage field, which does not resemble the response of many brittle materials, unless the internal length scale is made dependent on the local strain or stress [17], that in turn often results in additional computational costs [7]. On the other hand, rate dependent models have been proposed to solve mesh dependence keeping the strain at each material point independent of the nearby ones [3]. In general, this is done by implementing viscosity (rate dependent) functions directly in the governing equilibrium equations. Theoretically, the use of rate is still the most computationally efficient and physically consistent strategy to solve mesh dependency in the case of quasi brittle building materials sensitive to rate, such as concrete [5]. Unfortunately, only a limited number of these models proved to provide full regularization to damage models [5]. Using rate to restore ellipticity of the governing equations is a challenge especially in case of quasi-static simulations. This also counts for well known local regularization models [8]. A local damage model based on the last μ model for concrete structures [18] was recently developed by Pereira et al. [2] to simulate concrete. Among the conclusions, it was stated that rate functions within the equilibrium equations only have a weak regularization role and instead a nonlocal algorithm was supplemented [18].

In the current study, a numerical algorithm based on rate dependency is presented, which is integrated within the constitutive laws of the local model of [2], with the coupled aim of mesh regularization in statics and material property [19]. This is obtained by generalizing the concept of damage delay introduced by

Allix et al., in which a certain delay after damage initiation is defined while keeping its rate bounded [20, 21]. The generalization is based on a decomposition of the Dirichlet boundary conditions, which allows the parameters of the rate functions mathematically needed to regularize the model to be non-dimensional, and not necessarily time-dependent [22]. Thus, they can be calibrated from experimental tests performed in statics.

Many commercial software packages available nowadays use explicit solution schemes to approximate the solution of the partial differential equations of equilibrium at each step of a numerical simulation. They are easy to implement and computationally efficient but they need restricted time steps. On the contrary, besides harder implementation costs, only implicit solvers enforce equilibrium at each iteration, assuring robust and accurate evaluations of the state of the system. Thus, integration of equations of equilibrium of the regularized model has been implemented within a Newton-Raphson solver, which provides robustness to the resulting new algorithm. The model was called "Adobe delta damage model" because it has been applied for the static assessment of the mechanical performance of Adobe components.

Adobe is a traditional masonry whose bricks made of sundried mixtures of soil with reinforcing natural fibre are joined together using mud mortar [23]. As a consequence of a lack of knowledge on the physical-mechanical performance of Adobe, no adequate numerical models have been developed for Adobe and only a few attempts to numerically simulate the constitutive response of bricks and mortar of Adobe were found in literature [24]. This situation occurs because this building technology was progressively abandoned starting from industrial revolutions in favour of modern materials introduced in the construction market [25]. Nevertheless, in recent times Adobe has gained scientific interest, as a result of a specific socio-economic conjuncture [26]. Earthen buildings, which provide shelter to more than one third of the world population constituting 10% of the built heritage [27], are spread in areas of the world prone to natural hazards or involved into military operation, with the related treats for human beings and their property. Moreover, attractive thermal and acoustic material

properties make Adobe still a suitable building technology for Western countries involved within enviromental impact reduction tasks inherent building industry production processes [28]. Several experimental campaigns were performed by the authors on Adobe over the last five years, ranging from granulometry tests on soil mixtures to impact tests on walls [26, 29, 30]. The research led to the conclusions that Adobe can be regarded as a quasi brittle geomaterial of the same class as concrete, with a pronounced influence of soil granulometry on the overall mechanical performance [31, 32]. The new numerical model herein presented was adopted to simulate the static response of Adobe bricks and mortar subjected to uniaxial compression and three point bending tests in [26]. The Adobe delta damage model is presented in Section 2. Mesh objectivity of the model is demonstrated in Section 3. In Section 4, the model is applied to simulate the response of Adobe bricks and mortar in static tests performed by the authors in [26].

2. The Adobe delta damage model

The "Adobe delta damage model" is presented in this chapter. Implementation of the model starts from the classical formulation for isotropic damage in eq.(1) [33]:

$$\sigma = (1 - D)\tilde{\sigma} \quad \text{with} \quad \tilde{\sigma} = E : \varepsilon \ , \tag{1}$$

where $\tilde{\sigma}$ is the effective stress vector, ε is the strain vector, E the elastic stiffness tensor and D is the damage scalar, a parameter which ranges between 0 (integer material) and 1 (fully damaged material). Damage starts when the loading function f in eq.(2) becomes negative:

$$f = k_0 - \varepsilon_{eq} \ , \tag{2}$$

where ε_{eq} and k_0 are the equivalent strain and the damage initiation strain, respectively.

A modified Drucker-Prager damage loading surface is adopted in the model like in [2, 18]. Two equivalent strain functions for compression crushing (ε_{eq_c}) and tensile cracking (ε_{eq_t}) are expressed as a combination of the first (I_ε) and second deviatoric (J_{ε_d}) invariants of strain [34]. In eq.(3-4), they are presented within the octraedical space, as a combination of its normal (ε_{oct}) and tangential (γ_{oct}) components as in soil mechanics [35]:

$$\begin{cases} \varepsilon_{eq_t} = c_1\varepsilon_{oct} + c_2\gamma_{oct} \\ \varepsilon_{eq_c} = c_3\varepsilon_{oct} + c_4\gamma_{oct} \end{cases} \tag{3}$$

in which:

$$\begin{cases} \varepsilon_{oct} = \dfrac{1}{3}I_\varepsilon = \dfrac{\varepsilon_1 + \varepsilon_2 + \varepsilon_3}{3} \\ \gamma_{oct}^2 = -\dfrac{8}{3}J_{\varepsilon_d} = \dfrac{4}{9}[(\varepsilon_1 - \varepsilon_2)^2 + (\varepsilon_2 - \varepsilon_3)^2 + (\varepsilon_3 - \varepsilon_1)^2] \end{cases} \tag{4}$$

where subscripts $_{1,2,3}$ denote principal values of the strain tensor. Parameters $c_1 - c_4$ are defined as [18]:

$$\begin{cases} c_1 = \frac{1}{(1-2\nu)} \\ c_2 = \frac{1}{2\sqrt{2}(1+\nu)} \\ c_3 = \frac{3}{5(1-2\nu)} \\ c_4 = \frac{3\sqrt{3}}{5\sqrt{2}(1+\nu)} \end{cases} \tag{5}$$

where ν is the Poisson's ratio.

Evolution of damage is directly related to the growth of two monotonic internal variables which account for the historical maximum equivalent strains reached during loading history. They are implemented separately for compression (k_c) and tension (k_t) according to [36]:

$$\begin{cases} k_c(i) = \max[\ \varepsilon_{eq_c}(1 - r^{\alpha}), k_{0c}(\tau)] \quad \text{for all} \quad i \geqslant \tau \\ k_t(i) = \max[\ \varepsilon_{eq_t} r^{\alpha}, k_{0t}(\tau)] \quad \text{for all} \quad i \geqslant \tau \end{cases} \tag{6}$$

Where r is derived from the triaxiality factor proposed by Lee and Fenves [37] for multiaxial loading states, α is a constant set to 0.1 as in [2] and the mechanical parameters k_{0t} and k_{0c} are the damage initiation strains in tension and compression [34].

The value of damage in eq (1) combines two damage evolution laws in compression (D_c) and tension (D_t) as in [2], in which the respective equivalent strains enter:

$$D = 1 - (1 - D_c^{RD})(1 - D_t^{RD}) \tag{7}$$

where RD stands for rate dependent (regularized).

Both evolution laws in compression and tension start from rate independent softening functions generalized as combinations of exponential and linear softening showed in eq.(8) [2]:

$$(D)_{c,t}^{RI} = 1 - \frac{1}{e^{A_{c,t}(k_{c,t} - k_{0_{c,t}})}} - \frac{k_{0_{c,t}}}{B_{c,t} k_{c,t}} \tag{8}$$

Where A and B are material parameters and RI stands for rate independent. To address mesh dependence without introducing non locality in the model as in [36], the concept of bounded damage rate is adapted [22]. This consists of introducing a certain delay after local damage initiation while keeping the rate of damage bounded [38]. This is consistent with a finite velocity of propagation for material flaws [15]. Originally developed for composite laminates, the concept is considered to be suitable to address failure of quasi brittle materials used for masonry. In the model for adobe, the local damage evolution laws in compression and tension are then made directly dependent on the loading history based on a decomposition of the Dirichlet boundary condition. Given an arbitrary displacement law evaluated in N points by the Newton-Raphson solver, at each progressive step i of the analysis after damage initiation, both the loading evolution laws in compression and tension enter rate dependent functions (RD) according to eq. (9), in order to account for a "*delta*"(δ) increment based on the prescribed loading history:

$$D^{RD}_{c,t_i} = \delta D_{c,t_i} + D^{RD}_{c,t_{i-1}} \tag{9}$$

where the delta functions δD at each step are calculated using a function of exponential shape as in [20] modified according to eq.(10):

$$\delta D_{c,t_i} = \frac{\Delta_{c,t}}{N}(1 - e^{-(D^{RI}_{c,t_i} - D^{RD}_{c,t_{i-1}})}) \tag{10}$$

in which the Adobe delta damage model, Δ represents a further non-dimensional material parameter and N is needed to make the results independent of discretization of the applied law. The regularizing properties of the model come from the exponential damage-delay functions and will be demonstrated in Sec. 3.

The set of governing equations are integrated within an implicit Newton-Raphson solver. The code has been developed in C++ environment using the opensource libraries of JemJive [39].

3. Mesh Sensitivity Analysis

This chapter demonstrates the mesh objectivity of the "Adobe delta damage model" in statics. Four different tests commonly used in literature to diagnose the mesh sensitivity are adopted [3, 40]. The analysed tests are an uniaxially loaded tapered bar, a shear layer test, a shear band test and a cantiveler beam test in bending. They are used to verify the local damage distribution and the global reaction force plots for different levels of mesh refinement. The first two are classical tests from literature which analyse the unidirectional performance of the model. The latter two reproduce physical problems characterized by complex stress states.

Mesh dependence was analysed for wide ranges of variations of elastic (E, ν) and inelastic (Δ, A, B) parameters of the model in compression ($_c$) and tension ($_t$), consistently with ranges of mechanical values found in literature for Adobe [19] (Table 1). In the following paragraphs, examples of results obtained from specific combinations are shown for each test.

Four node plane stress elements are used in the model. A value of N=2000 and a precision of $10e^{-5}$ is prescribed to the implicit solver.

3.1. ***Uniaxially loaded tapered bar test***

A classical test from theory widely used to diagnose mesh dependence is the tapered cantilever bar uniaxially loaded [3]. The response of a tapered bar to uniaxial compression is analysed. A displacement is applied at the free edge of a 100mm long bar fixed at the bottom (Figure 1). In order to trigger localization, a 3% tapering is applied along the height of the bar starting from 1mm thickness. The mesh of the bar is progressively refined starting from 10 up to 160 elements. The results of this analysis for progressive mesh refinement are shown in the following in terms of global reaction-displacement plots (Figure 2) and local damage profiles along the bar (Figure 3). They correspond to the following set of values inserted as mechanical parameters of the model: A_c=60, B_c=0, Δ_c = 5, ν =0.0, E=150 MPa, k_{0_c}=1.0%.

Force displacement plots nearly overlap, with maximum relative errors lower

than 1% (Figure 4(a)), while the damage profile is consistent for all meshes during the entire simulation (Figure 4(b)).

Analysis of results yields the conclusion that the model is capable of producing mesh independent simulations and good results are obtained already with the coarsest mesh. For explanatory purposes, the performance of the Adobe delta damage model is compared with respect to the corresponding rate independent version. Results confirm the numerical pathology of the local model. The damage distribution and force displacement plots depict a not-consistent progressively more brittle behaviour upon mesh refinement (Figure 5).

3.2. ***Shear layer test***

Another test performed to verify mesh dependence is the shear layer transversally loaded (Figure 6) [41, 10]. The response of the model in pure shear is analysed. A thick column fixed at its bottom and constrained vertically along the height is subjected to a shear load at the free edge at the top. The set up is given in Figure 6. In order to trigger localization, a mechanical imperfection is inserted along the first 10mm of the beam in terms of a 15% decrease of the damage initiation strain. The mesh of the shear column is progressively refined starting from 10 elements up to 160.

The results for progressive mesh refinement are shown in Figure 7(a) in terms of overall reaction-displacement plots and in Figure 7(b) in terms of failure damage profile along the bar. They correspond to the following set of mechanical parameters of the model: A_c=100, B_c=0, A_t=0, B_t=100, $\Delta_c = 6$, $\Delta_t = 6$, ν =0.0, E=200 MPa, k_{0_c}=0.6%, k_{0_t}=0.6%. Force displacement plots nearly overlap and the damage profiles match for the different meshes.

The analysis is mesh independent and good results are obtained already for the coarsest mesh.

3.3. ***Shear band test***

Specimens under compression are usually characterized by the formation of shear bands. The mesh objective determination of shear bands is of primary

interest [42]. A constrained cube of 50x50mm is compressed at the top in Figure 8. A shear band is triggered by a mechanical imperfection introduced by a 30% reduction of the damage initiation strain, in the left bottom corner in the grey region in Figure 8. The first mesh is chosen to have one element included in the weakest region and progressive mesh refinement is adopted.

The results of the mesh refinement analysis are shown in the following in terms of reaction-displacement plots (Figure 9(a)) and failure damage distribution within the specimen (Figure 9(b)). They correspond to the following set of values inserted as mechanical parameters of the model: A_c=250, B_c=0, A_t=0, B_t=100, $\Delta_c = 9$, $\Delta_t = 9$, ν =0.1, E=200 MPa, k_{0_c}=0.7%, k_{0_t}=0.2%.

Also in a shear band test, the model is capable of performing simulations in a mesh objective manner.

3.4. ***Cantilever beam in bending***

The last test verifies the numerical response of the model in bending. A slender cantilever beam (L/b=4) is subjected to a distributed transversal load at the free edge (Figure 10). Due to the stress distribution, neither a geometrical nor a mechanical imperfection is used to trigger localization.

Results using the same mesh refinements as in the shear band test are demonstrated in terms of reaction-displacement plots (Figure 11(a)) and failure damage distribution within the specimen (Figure 11(b)). They correspond to the following set of values inserted as mechanical parameters of the model: A_c=500, B_c=5, A_t=500, B_t=0, $\Delta_c = 6$, $\Delta_t = 6$, ν =0.1, E=350 MPa, k_{0_c}=0.4%, k_{0_t}=0.2%.

Mesh objectivity is again confirmed.

3.5. ***Parameter sensitivity analysis***

This paragraph briefly presents a parameter sensitivity analysis of the model. The uniaxially loaded tapered bar presented in Sect. 3.1 is used for variation of the parameter A for the same mesh of 20 elements (Figure 12 (a-b)). The original parameter A=60 is doubled and halved. Similary, results of an analysis using

half and double values of the original Δ=5 are presented in (Figure 12 (c-d)). From both analyses, it is evident that by increasing the values of the numerical parameters, brittleness is enhanced demonstrated by a steeper softening post-peak branch and more localized damage. This effect is more pronounced for a variation of A than for Δ (Figure 12 (e-f)).

All analyses confirmed to be mesh independent already for the coarsest discretization (Figure 13 (a-b)). The only noticible difference is related to the initial jump in maximum force and displacement at peak load errors with respect to the first level of mesh refinement, which is more pronounced for higher values of Δ or lower values of A; nevertheless all errors are significantly lower than 1%.

4. A numerical application of the Model on Adobe

4.1. The Experimental reference

Once mesh objectivity of the model has been proven, numerical simulations are performed in order to verify the suitability of the framework for the assessment of the mechanical response of Adobe components in statics. A physical-mechanical characterization campaign performed by the authors on unfired soil bricks (which are fiber reinforced) and mortar (fiber free) is chosen as experimental reference [26]. It consisted of compressive and bending tests on four types of bricks and one mortar characterized by different percentages of fiber reinforcements [26]. Displacement controlled tests at very low rate (1 mm/min) were performed on prisms with a slenderness equal to two in unixial compression or on entire bricks in bending. Interpretation of results led to the conclusion that Adobe components belong to the material class of concrete [31].

The typical force-displacement diagram in compression shows three distinct phases (Figure 14(a)). The initial behaviour is linear-elastic and the brick is supposed to be intact. At a stress level between 60% (typically for adobe bricks) and 75% (mainly for mortar samples) of the compressive strength, pre-peak non linearity is observed. This is the likely consequence of the coalescence and development of micro cracking processes occurring inside the sample. After peak load, diagonal and vertical macro-cracks are visible at opposite edges; correspondingly softening behaviour is observed in the force displacement curve, while cracks spread over the whole sample with a conical pattern (Figure 14(b)). When the soil matrix is mixed with fiber, the behaviour of Adobe becomes more ductile. Pre-peak non linearity starts at lower strain levels, while values for strain at peak load increase, as well as the slope of the post-peak slope of softening [26].

A more brittle behaviour characterizes the mechanical response of Adobe in bending. The typical force-displacement diagram is linear until 95% (bricks) or 98% (mortar) of the peak load is reached (Figure 14(c)). A single crack is then immediately visible at the lateral surfaces of the mid span and a corresponding

softening branch in the force diagrams with typical exponential shape is obtained (Figure 14(d)). The crack propagates quickly along the height, and at 50% of the peak load, it reaches a relative length (with respect to the height of the sample) of approximately 45% (bricks) and 52% (mortar). Also in bending, strain at peak stress and slope of the softening curve are dominated by the fiber amount in the mixture.

4.2. The numerical hypotheses of the model

Numerical simulations were performed for all types of adobe experimentally tested in [26]. In the following, numerical simulations using the new model are shown for one type of brick (reinforced using 17% by weight of straw in the mixture and named "Brick" in the following) and one type of mortar with only little traces of organic content (named "Mortar" in the following).

Assumptions for the material parameters of the model and simulation goals are made:

- For the Young's modulus, the mean values of elastic stiffness experimentally derived in [26] for Brick (E = 100 MPa) and Mortar (E= 200 MPa) are used. A 0.1 value for the Poisson's ratio is assumed, which is equal to the value used in the only known research devoted to the determination of this material parameter for Adobe [25];

- Consistently with the hypotheses of a new phenomenological model recently developed by the authors to address the ballistic resistance of Adobe [32], the Drucker Prager surface of eq.(2) in Sec.2 used in [19] is updated to include an inscribed Drucker Prager smoothed version of Mohr Coloumb failure in compression (Figure 15(a)). In the octraedical space used in Sec.2, this implies the modification of the set of parameters c_1-c_4 of the equivalent strain formulations as follows:

$$\begin{cases} c_1 = \frac{1}{(1-2\nu)} \\ c_2 = \frac{1}{2\sqrt{2}(1+\nu)} \\ c_3 = \frac{tg(\phi)}{(1-2\nu)} \\ c_4 = \frac{\sqrt{3}}{2(1+\nu)} \end{cases} \tag{11}$$

  in which the internal friction angle ϕ=10^o is chosen corresponding to organic soil [43].

- For the damage initiation strains in compression, the mean values of initial deviation from linearity in the averaged stress strain diagrams experimentally derived in [26] are used for Brick (k_{0_c} = 1.3%) and Mortar (k_{0_c} =

0.7%). Elastic stiffness and initial damage strain in tension are determined in agreement with the sigma-epsilon method of the RILEM standard for fibre reinforced concrete [44]. Symmetry in elastic slope in tension and compression is thus hypothisezed and as damage initiation strain in tension, the mean value of strain corresponding to the formation of the first crack in bending tests experimentally derived in [26] is used for Brick (k_{0_t} = 0.7%) and Mortar (k_{0_t} = 0.3%).

- The damage evolution laws in eq. 7 are simplified. Different functions are used for compression and tension (Figure 15(b)). A steeper linear softening is adopted for tension while a smoother exponential shape is chosen for compression consistently with experimental trends of Par. 4.1. The resulting damage evolution laws are:

$$\begin{cases} D_c = 1 - \dfrac{1}{e^{C(k_c - k_{0c})}} \\ D_t = 1 - \dfrac{k_{0t}}{T k_t} \end{cases} \tag{12}$$

- Mean approximate dimensions are used for Brick and Mortar (Figure 16(a)) taken from [26]. In bending, the imposed interspan and the size of the distribuited constraining rolls are kept equal to experiments (Figure 16(b)). In order to trigger localization, in compression a mechanical defect, with damage initiation strain equal to 0.1%, is imposed at the corners of the specimen. Because of symmetry, only half of the brick is meshed. In bending a geometrical imperfection is used and a quadrilateral 1mm mesh with four integration points is applied. Displacement controlled analyses with small incremental steps ($5*10^{-4}$) are imposed at the upper side of the sample in compression and at the mid span in bending. A precision of $1*10^{-5}$ is prescribed to the solver.

- Calibration of parameters C, T, Δ in compression is performed in order to interpolate as closely as possible the mean displacements at peak stress and

the 90% pre and post peak (named ultimate displacement in [26]) strength decay experimentally derived in [26] for Brick and Mortar. Calibration of damage function parameters in tension is performed in order to match as closely as possible the mean slope of the post peak exponential softening curve experimentally derived in [26] for Brick and Mortar. All material parameters used in compression are taken the same for bending tests. For sake of simplicity, the value of Δ is initially assumed constant for Brick and Mortar in tension and compression.

4.3. ***The numerical results and comparisons with experiments***

The best fit simulations in compression and bending are shown for Brick and Mortar in Figure 17. They are presented together with the targeted mean experimental plots associated to each type. Both curves are inserted within the minimum and maximum envelopes of experimental data related to compressive and bending tests on bricks and mortar. The corresponding failure patterns are compared in Figure 18.

In compression, the numerical results match the experimental data well at least until ultimate displacements for both Brick and Mortar in Figure 17(a-b). As a result of the simple formulation of eq.12, the numerical reaction plots do not capture the experimental trends of the post-peak experimental regions for large displacements (which could be experimentally recorded only for a limited number of specimens). Differences may be due to a more distributed failure pattern in the tests due to material heterogeneity which can not be addressed using deterministic models. Advanced softening laws with more ductility in the final failure stage may also provide a better match between test and simulation. Nevertheless, the numerical curves lie within the experimental envelopes associated to bricks and mortar at least up to 50% of the post peak stress.

The numerical failure resembles the principal experimental cracking patterns depicted for Adobe in Par. 4.1, despite the simplifications as two-dimensional modelling, isotropy and setup of the model to simulate developments of cracks usually starting from fiber-induced areas of de-adherence, clay concentrations

or defects [26](Figure 18(a)).

Also for three point bending tests it was possible to accomplish the goal and the numerical f-d plots match most of the elastic and post peak softening experimental curves for both Brick and Mortar (Figure 17(c-d)). Also here a slight deviation between experiment and simulation is observed in the later stage of loading. However, also in bending the numerical plots remain within the experimental envelope for values higher than 50% of the post peak stress. Moreover, using the material parameters derived in compression and the flexural strain as given in RILEM for concrete, the resulting values of tensile strength derived from eq.(13) well approximate the strength values experimentally derived in [26] for both components (Figure 19(b)).

$$f_t = \frac{3F_{max}s}{2th^2} \tag{13}$$

where the peak load (F_{max}) and the displacement at peak load ($d_{F_{max}}$) with the geometrical dimensions in thickness (t), height (h) and span (s) are input from numerical results.

Almost full resemblance is extended to the depiction of the failure mode, where a single crack starts after damage initiation and it propagates quickly along the heigth (Figure 18(b)). Match with experiments is quantitatively extended to the evaluation of the cracking rate, meant as the ratio between length and height with respect to the same decay of strength after peak load (Figure 19(a)).

4.4. ***A physical interpretation of numerical calibration***

The material parameters used for calibration are listed in Table 2. In compression it was possible to keep Δ_c constant for Brick and Mortar, while the brittle curves in bending required the use of a very high value for T for Adobe components, leaving Δ_t as calibrating parameter. Calibration of numerical parameters is qualitatively consistent with observed experimental trends [26]. Given a fixed value for Δ_c, the difference in value of the material parameter C, higher for Mortar than Brick, is consistent with the experimental evidence that mixtures

with higher fiber content show higher ductility in compression. They are shown in Figure 20 (a), where the material parameter C for Brick and Mortar is given as function of the corresponding reinforcement ratio. The calibration of parameter C for all types of bricks tested was performed in [19]. A similar trend is shown for parameter Δ_t in tension (Figure 20 b).

5. Conclusions

A rate-dependent damage model has been developed to numerically assess the material performance of Adobe masonry components in statics. It originates from a local model recently developed for concrete with limiting regularization properties. In this study, the numerical model has been made fully mesh objective in statics, integrating rate dependent damage functions within an implicit solution scheme. The resulting rate dependent model assures mesh independence within a robust algorithm prone to preserve coherence with the physics of quasi brittle materials. A decomposition of the Dirichlet boundary condition allows all the numerical parameters of the damage evolution laws to be non dimensional. Thus, they could be calibrated with respect to the static experimental results in compression and bending of one type of brick and mortar experimentally tested by the authors. Despite simplicity, the current version of the model could cover the main features of the experimental response of components in compression and tension. Therefore it constitutes a valid framework to numerically assess the mechanical performance of Adobe components and the modified Drucker Prager failure surface is confirmed to well addresses the material response in compression.

List of Tables and Figures

Table 1: Ranges of tested values using the "Adobe delta Damage Model" for mesh sensitivity analysis

Parameter	**Value**	**Parameter**	**Value**
E, E_t	10-250 MPa	$A_{c,t}, B_{c,t}$	25-1000
k_{0c}, k_{0t}	0.3-1.5%	$\Delta_{c,t}$	3-500
ν	0.0-0.15	$\frac{k_{0d}}{k_0}$	10-30%

Table 2: Best fit material parameters in compression and tension for Brick and Mortar

Type	C	Δ_c	T	Δ_t
Brick	140	5.0	1000	160
Mortar	180	5.0	1000	440

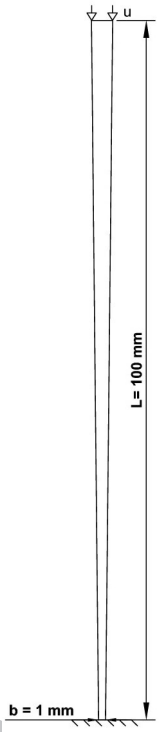

Figure 1: Setup for mesh sensitivity study for the uniaxially loaded tapered bar test: geometry and boundary conditions

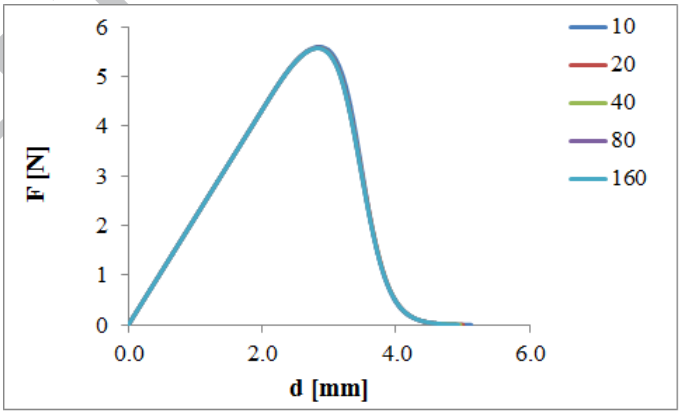

Figure 2: Force-displacement diagrams for progressive mesh refinement for the uniaxially loaded tapered bar test

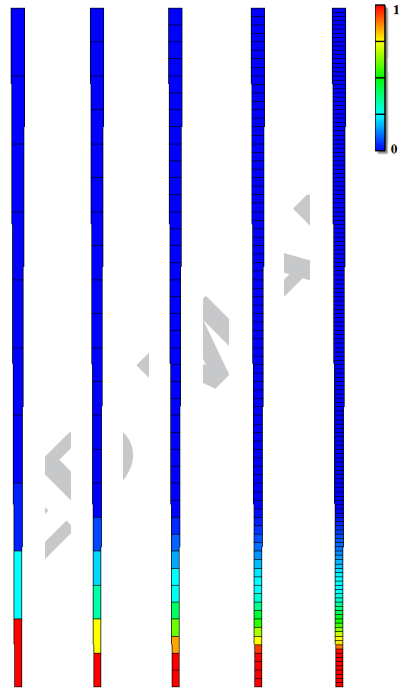

(a) (b) (c) (d) (e)

Figure 3: Damage profile for progressive mesh refinement for the uniaxially loaded tapered bar test at d=4.0mm

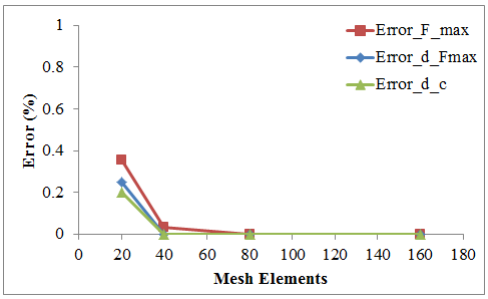

(a)

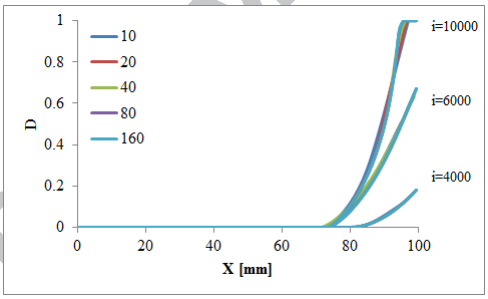

(b)

Figure 4: Relative errors in terms of maximum reaction force (F_{max}), displacement at peak load ($d_{F_{max}}$) and strain at 20% decay of reaction (d_c) for different mesh elements (a) and damage profile along the bar at different stage of simulations (i) (b)

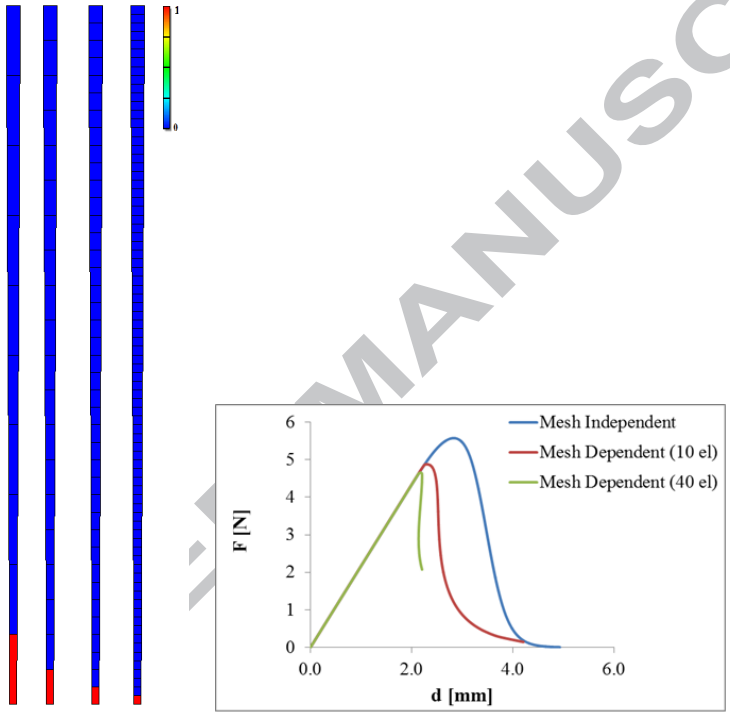

(a) (b)

Figure 5: Damage profile for progressive mesh refinement for the uniaxially loaded tapered bar test using the rate independent local model (a) and comparisons of force-displacements graphs for progressive mesh refinement with respect to mesh independent solution (b)

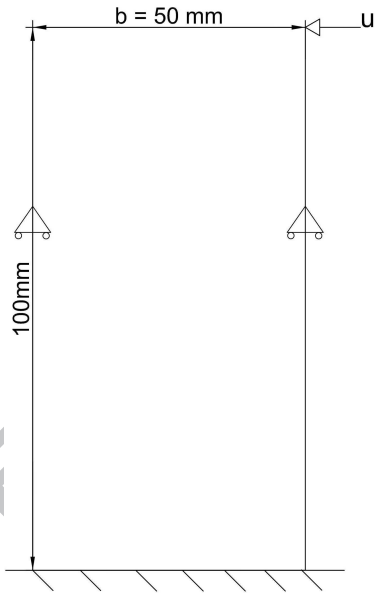

Figure 6: Setup for mesh sensitivity study for the shear layer test: geometry and boundary conditions

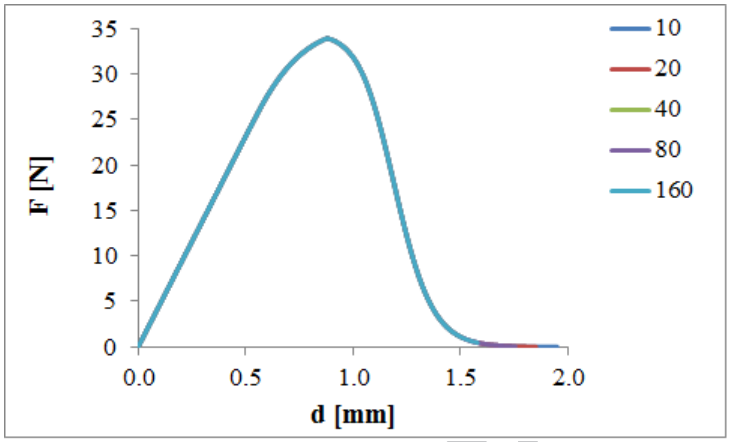

(a)

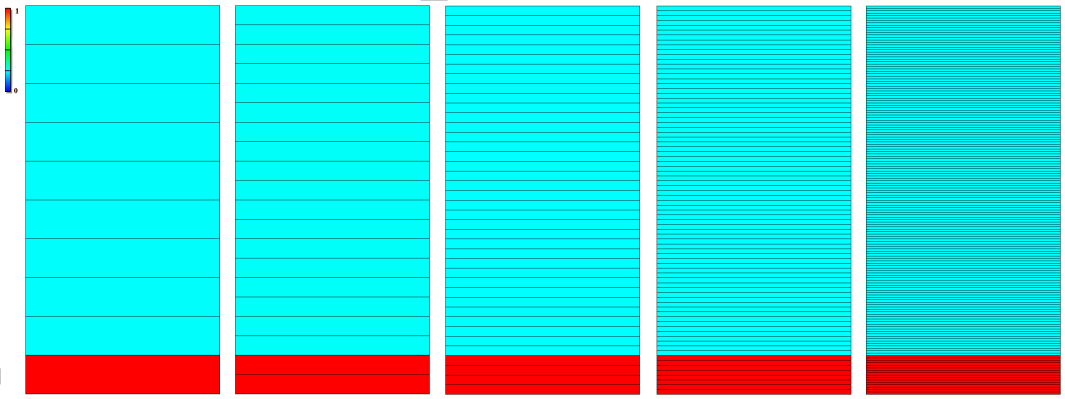

(b)

Figure 7: Force displacement (a) and damage profile at d = 1.5 mm (b) for progressive mesh refinement for the shear layer test

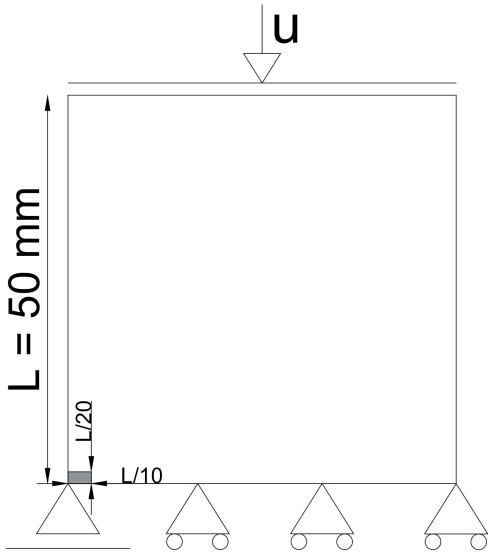

Figure 8: Setup for mesh sensitivity study for the shear band test: geometry and boundary conditions

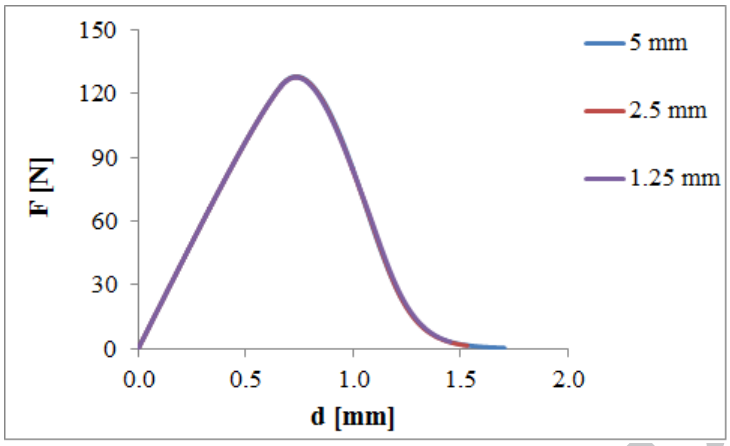

(a)

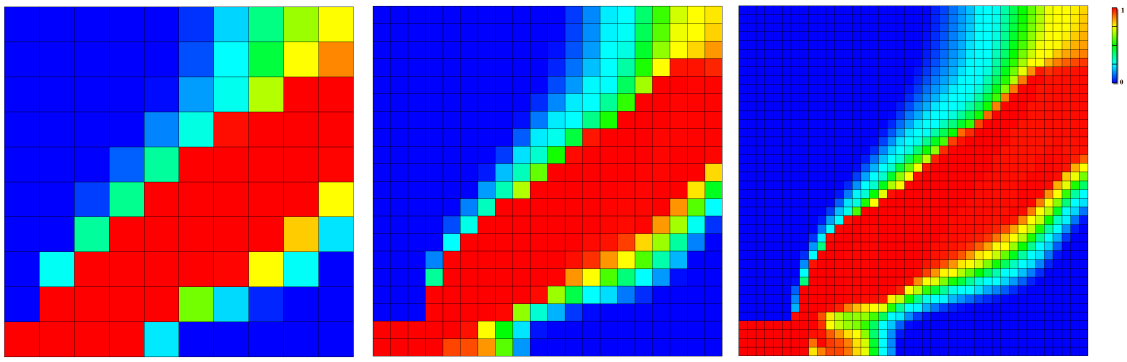

(b)

Figure 9: Force displacement (a) and damage profile at d = 1.3 mm (b) for progressive mesh refinement in the shear band test

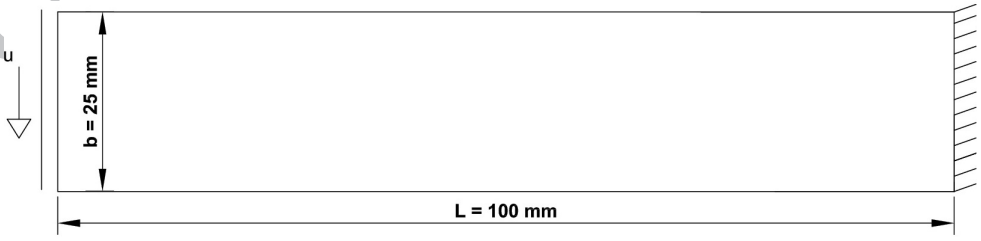

Figure 10: Setup for mesh sensitivity study for the cantilever bending test: geometry and boundary conditions

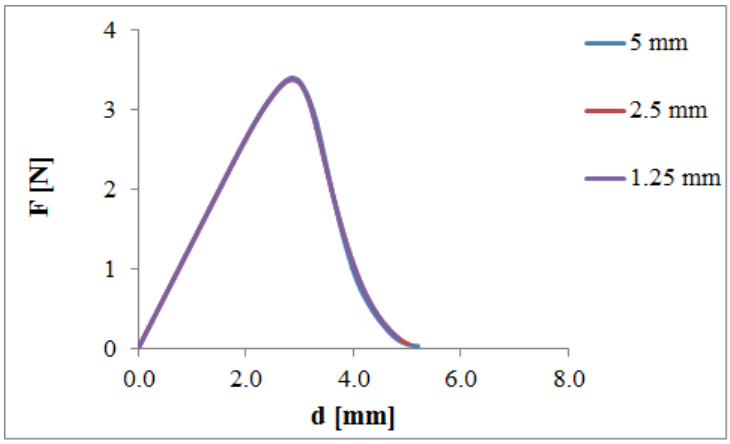

(a)

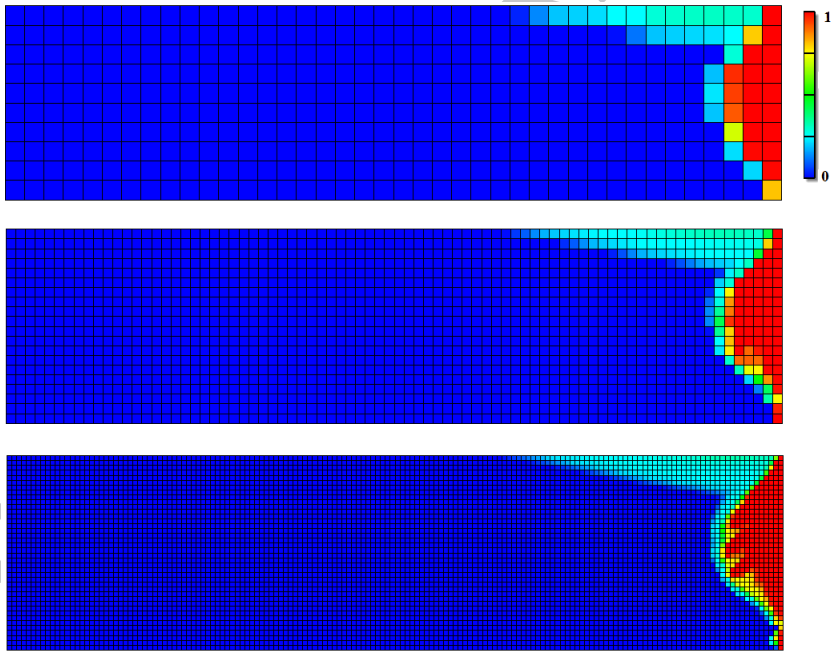

(b)

Figure 11: Force displacement (a) and damage profile at d = 4.3 mm (b) for progressive mesh refinement in the cantilever bending test

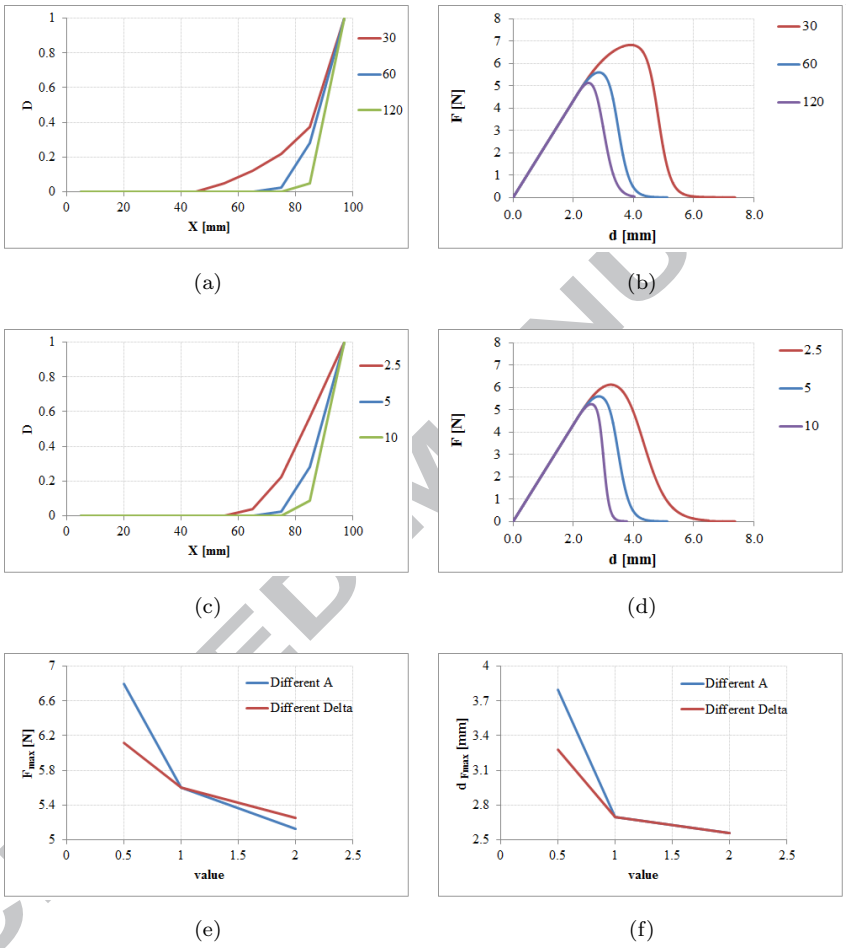

Figure 12: Damage profile in the bar (a,c) and force displacement plots (b,d) varying values of A (a-b) or Δ (c-d) and comparison of the variation of response in terms of maximum force (e) and displacement at peak force (f)

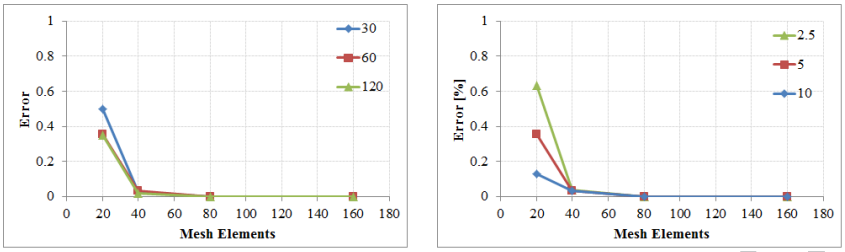

(a) (b)

Figure 13: Error comparison for progressive mesh refinements using half and double A (a) or Δ (b)

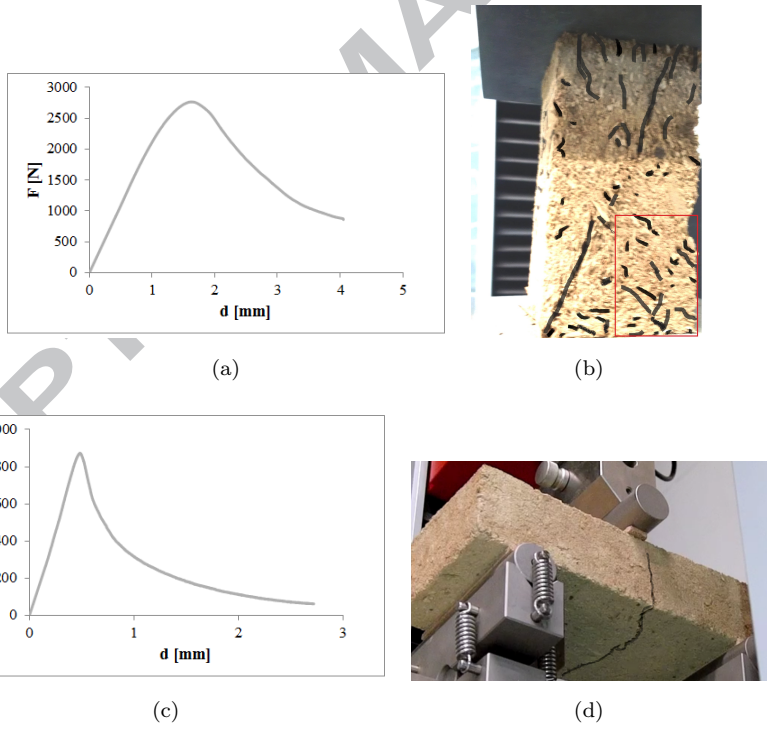

(a) (b)

(c) (d)

Figure 14: *Typical regions of the F-d diagrams and related cracking patterns in compression (a-b) and bending(c-d)*

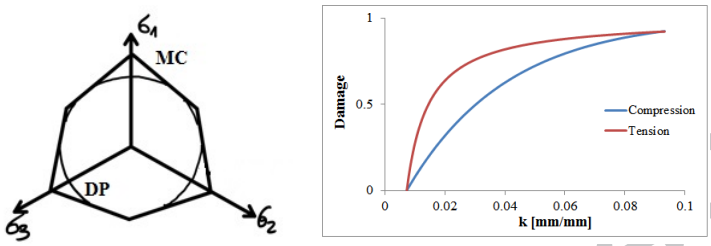

(a) (b)

Figure 15: Smoothed Drucker-Prager damage surface (DP) of the Mohr-Coulomb (MC) failure used in compression (a) and damage profiles in tension (T=1) and compression (C=30) (b)

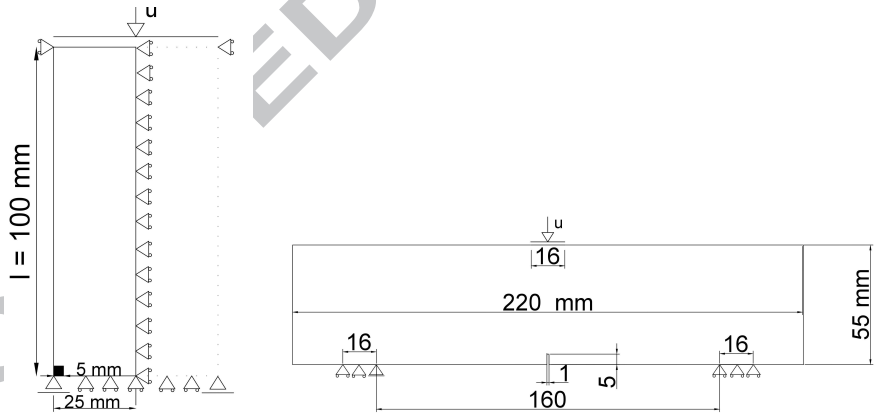

(a) (b)

Figure 16: Numerical setup in compression (a), and three point bending test (b), including geometry and boundary conditions

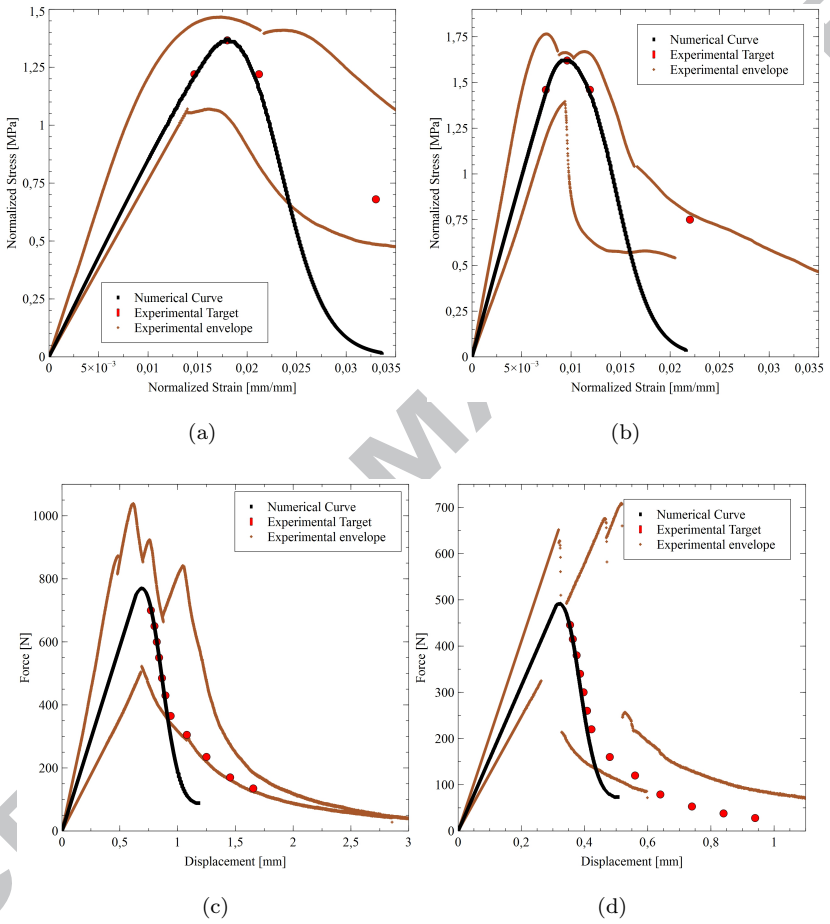

Figure 17: Experimental-Numerical force-displacement comparisons in compressions (a-b) and flexure (c-d) for Brick (left) and Mortar (right)

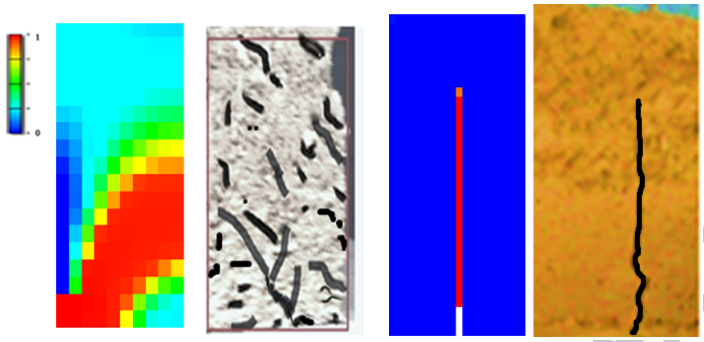

(a) (b)

Figure 18: *Experimental-Numerical comparison in terms of failure pattern in compression of Brick with quarter of CA11a (brick) at about 2mm (a) and in bending at mid span of Mortar with M3 (mortar) at a decay of about 20% of the strength (b)*

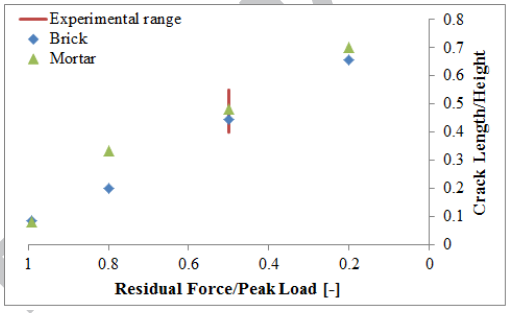

(a)

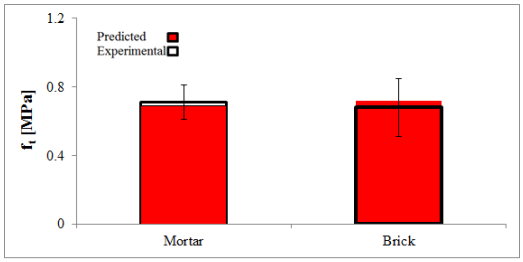

(b)

Figure 19: *Experimental-Numerical comparison in terms of crack propagation in bending (a) and in terms of tensile strength evaluation (b) for Brick and Mortar*

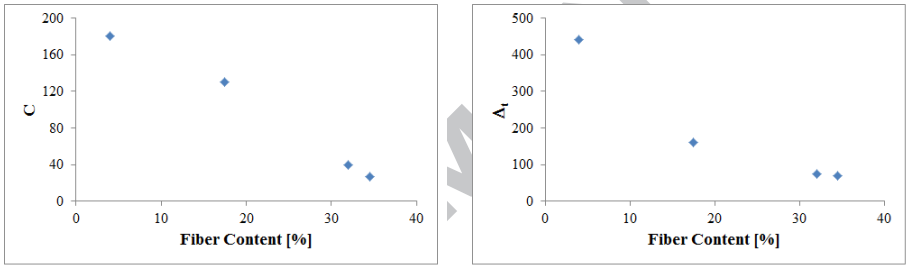

(a) (b)

Figure 20: Relationships between *calibrated* material parameters of the numerical model and experimental fibre content for four different types of bricks and mortar (including Brick and Mortar) tested in [26]

References

[1] T. Li Piani, Operative Guidelines for Protection of Places of Worship: A new approach toward security design of sensitive buildings, Institute for Advanced Strategic and Political Studies (IASSP), Milan, 2017.

[2] L. F. Pereira, J. Weerheijm, L. J. Sluys, A new effective rate dependent damage model for dynamic tensile failure of concrete, Engineering Fracture Mechanics 176 (2017) 281–299. doi:10.1016/j.engfracmech.2017.03.048.
URL http://linkinghub.elsevier.com/retrieve/pii/S001379441630474X

[3] L. J. Sluys, R. de Borst, Wave propagation and localization in a rate-dependent cracked medium-model formulation and one-dimensional examples, International Journal of Solids and Structures 29 (23) (1992) 2945–2958. doi:10.1016/0020-7683(92)90151-I.

[4] P. Grassl, M. Jirásek, On mesh bias of local damage models for concrete, Proc., 5th Int. Conf. on Fracture Mech. of Concrete Structures (FraMCoS-5) (5) (2004) 255–262.

[5] L. J. Sluys, R. De Borst, Mesh-sensitivity analysis of an impact test on a double-notched specimen, Rock Mechanics, 1991.

[6] L. J. Sluys, R. De Borst, Rate dependent modelling of concrete fracture, Heron 36(2), 3-16. (1991).

[7] M. Jirasek, Z. Bazant, Model for Localization of Softening and Size Effect, in: Inelastic Analysis of Structures, 2002, Ch. 26.

[8] A. Needleman, Material rate dependence and mesh sensitivity in localization problems, Computer Methods in Applied Mechanics and Engineering 67 (1) (1988) 69–85. doi:10.1016/0045-7825(88)90069-2.

[9] F. van der Meer, L. J. Sluys, Continuum Models for the Analysis of Progressive Failure in Composite Laminates, Journal of Composite Materials 43 (20) (2009) 2131–2156. doi:10.1177/0021998309343054.
URL http://jcm.sagepub.com/cgi/doi/10.1177/0021998309343054

[10] F. Meftah, J. M. Reynouard, O. Merabet, Localisation and mesh sensitivity in gradient dependent softening plasticity, Fracture Mechanics of Concrete Structures, Proceedings FRAMCOS-2, edited by Folker H. Wittmann, Aedificatio Publishers, D-79104 Freiburg (1995) 1069–1078.

[11] M. Jirasek, Regularized continuum damage formulations acting as localization limiters, in: Computational Modelling of Concrete and Concrete Structures: EURO-C 2018, CRC Press, Bad Hofgastein (Austria), 2018, pp. 25–43.

[12] O. Allix, P. Feissel, Composite Damage Model For Dynamic Fracture Prediction : Identification Issues, ICF 11-11th International Conference on Fracture 2005.

[13] G. Pijaudier-Cabot, Z. Bazant, Nonlocal damage theory, Engineering Mechanics 113 (10) (1988) 1512–1533.

[14] Z. P. Bažant, Fracture mechanics of concrete structures, ACI Committee 446 on Fractures Mechanics 140 (1992) (1992) 1–140.
URL http://www.civil.northwestern.edu/people/bazant/PDFs/Papers/S25.pdf

[15] O. Allix, The bounded rate concept: A framework to deal with objective failure predictions in dynamic within a local constitutive model, International Journal of Damage Mechanics 22 (6) (2012) 808–828. doi:10.1177/1056789512468355.
URL http://ijd.sagepub.com/cgi/doi/10.1177/1056789512468355

[16] C. Giry, F. Dufour, J. Mazars, Stress-based nonlocal damage model, In-

ternational Journal of Solids and Structures 48 (25-26) (2011) 3431–3443. doi:10.1016/j.ijsolstr.2011.08.012.

[17] R. de Borst, C. V. Verhoosel, Gradient damage vs phase-field approaches for fracture: Similarities and differences, Computer Methods in Applied Mechanics and Engineering 312 (2016) 78–94. doi:10.1016/j.cma.2016.05.015.

[18] J. Mazars, F. Hamon, S. Grange, A new 3D damage model for concrete under monotonic, cyclic and dynamic loadings, Materials and Structures (2015) 3779–3793doi:10.1617/s11527-014-0439-8.
URL http://link.springer.com/10.1617/s11527-014-0439-8

[19] T. Li Piani, J. Weerheijm, L. Koene, L. J. Sluys, The Adobe Delta Damage Model, in: Computational Modelling of Concrete Structures (EURO-C 2018), CRC Press, Bad Hofgastein (Austria), 2018, pp. 921–932.

[20] P. Ladevèze, O. Allix, J. F. Deü, D. Lévêque, A mesomodel for localisation and damage computation in laminates, Computer Methods in Applied Mechanics and Engineering 183 (1-2) (2000) 105–122. doi:10.1016/S0045-7825(99)00214-5.

[21] O. Allix, J.-F. Deu, Delayed-Damage Modelling for Fracture Prediction of Laminated Composites under Dynamic Loading, Engineering Transactions 45 (1).
URL http://et.ippt.gov.pl/index.php/et/article/view/680

[22] A. Suffis, T. A. A. Lubrecht, A. Combescure, Damage model with delay effect analytical and numerical studies of the evolution of the characteristic damage length, International Journal of Solids and Structures 40 (13-14) (2003) 3463–3476. doi:10.1016/S0020-7683(03)00153-7.

[23] R. Coffman, N. Agnew, G. Austin, E. Doehne, Adobe mineralogy: characterization of adobes from around the world, 6th International Conference

on the Conservation of Earthen Architecture, Las Cruces, New Mexico, U.S.A., October 14-19, 1990 1 (May) (1990) 424–429. doi:0892361816.

[24] R. Illampas, D. C. Charmpis, I. Ioannou, Finite Element Simulation of the Structural Response of Adobe Masonry Buildings Subjected To Lateral (October) (2014) 14–17.

[25] D. Silveira, Al., Mechanical properties of adobe bricks in ancient constructions, Construction and Building Materials 28 (1) (2012) 36–44. doi:10.1016/j.conbuildmat.2011.08.046.
URL http://dx.doi.org/10.1016/j.conbuildmat.2011.08.046

[26] T. Li Piani, D. Krabbenborg, J. Weerheijm, L. Koene, L. J. Sluys, The Mechanical Performance of Traditional Adobe Masonry Components: An experimental-analytical characterization of soil bricks and mud mortar, Journal of green building 13 (3) (2018) 17–44.

[27] World Heritage Earthen Architecture Programme (WHEAP), United Nation: Inventory of earthen architecture (2012).

[28] G. Minke, Building with earth: Design and Technology of a sustainable architecture, BirkhauserarXiv:arXiv:1011.1669v3, doi:10.1017/CBO9781107415324.004.

[29] T. Li Piani, J. Weerheijm, L. Koene, L. J. Sluys, The Ballistic Resistance of Adobe Masonry : An analytical model for impacts on mud bricks and mortar, in: The 17th International Symposium on the Interaction of the Effects of Munitions with Structures (17th ISIEMS), no. October, Bad Neuenahr, Germany, 2017.

[30] Resultaten miniMOUT: effect van veroudering op ballistische weerstand van adobe muren met twee steensterkten, TNO Report, Tech. rep., TNO (2013).

[31] T. Li Piani, J. Weerheijm, L. Koene, L. J. Sluys, Modelling the Mechanical Response of Adobe Components under Uniaxial Loading, Key Engineering Materials 774 (2018) 650–657.

[32] T. Li Piani, J. Weerheijm, L. J. Sluys, Ballistic model for the prediction of penetration depth and residual velocity in Adobe: A new interpretation of the ballistic resistance of earthen masonry, Defence Technology 14 (5) (2018) 4–8. doi:10.1016/j.dt.2018.07.017.
URL https://doi.org/10.1016/j.dt.2018.07.017

[33] J. Lemaitre, J. Chaboce, Mechanics of Solid materials, 1990.

[34] L. Pereira, J. Weerheijm, L. J. Sluys, Simulation of dynamic behaviour of quasi brittle materials with new rate dependent damage model, in: 9th International Conference on Fracture Mechanics of Concrete and Concrete Structures (FraMCos-9), 2015, p. 14. doi:10.21012/FC9.036.

[35] R. Lancellotta, Geotechnical engineering, 2nd Edition, CRC Press, 2008.

[36] L. F. Pereira, J. Weerheijm, L. J. Sluys, A new rate-dependent stress-based nonlocal damage model to simulate dynamic tensile failure of quasi-brittle materials, International Journal of Impact Engineering 94 (2016) 83–95. doi:10.1016/j.ijimpeng.2016.04.002.
URL http://dx.doi.org/10.1016/j.ijimpeng.2016.04.002

[37] J. Lee, G. L. Fenves, Plastic-Damage Model for Cyclic Loading of Concrete Structures, Journal of Engineering Mechanics 124 (8) (1998) 892–900. doi:10.1061/(ASCE)0733-9399(1998)124:8(892).
URL http://dx.doi.org/10.1061/(ASCE)0733-9399(1998)124:8(892){%}5Cnhttp://ascelibrary.org/doi/pdf/10.1061/(ASCE)0733-9399(1998)124:8(892)

[38] P. Ladevèze, A damage computational approach for composites: Basic aspects and micromechanical relations, Computational Mechanics 17 (1995) 4–15. doi:10.1007/BF00356486.

[39] V. P. Nguyen, Multiscale failure modelling of quasi-brittle materials. Manual to the implemented jem/jive code, Ph.D. thesis, Delft University of Technology (2011).
URL https://repository.tudelft.nl/islandora/object/uuid{%}3A1af168bf-7975-4044-8eb4-dd42216f7aaf

[40] G. Pijaudier Cabot, Z. P. Bažant, M. Tabbara, Comparison of various models for strain softening, Engineering Computations 5 (2) (1988) 141–150. doi:10.1108/eb023732.
URL http://www.emeraldinsight.com/doi/10.1108/eb023732

[41] E. C. Simons, J. Weerheijm, L. J. Sluys, A viscosity regularized plasticity model for ceramics, European Journal of Mechanics 72 (July 2017) (2018) 310–328. doi:10.1016/j.euromechsol.2018.05.009.
URL https://doi.org/10.1016/j.euromechsol.2018.05.009

[42] A. Simone, H. Askes, L. J. Sluys, Incorrect initiation and propagation of failure in non-local and gradient-enhanced media, International Journal of Solids and Structures 41 (2) (2004) 351–363. doi:10.1016/j.ijsolstr.2003.09.020.

[43] Swiss Standard SN 670 010b, Characteristic Coefficients of soils, Association of Swiss Road and Traffic Engineers.

[44] RILEM TC 162-TDF: Test and design methods for steel fibre reinforced concrete. Sigma-epsilon design method. Final Recommendation.